



# Distribution of strontium isotopes in river waters across the Tarim Basin: a map for migration studies

Xueye Wang<sup>1,2,3\*</sup>, Zihua Tang<sup>1,2,4\*</sup> & Xinxin Dong<sup>5</sup>

<sup>1</sup> Key Laboratory of Cenozoic Geology and Environment, Institute of Geology and Geophysics, Chinese Academy of Sciences, Beijing 100029, China

<sup>2</sup> Institutions of Earth Science, Chinese Academy of Sciences, Beijing 100029, China

<sup>3</sup> University of Chinese Academy of Sciences, Beijing 100049, China

<sup>4</sup> CAS Center for Excellence in Life and Paleoenvironment, Beijing 100044, China

<sup>5</sup> Bureau of General Affairs, Chinese Academy of Sciences, Beijing 100864, China

X.W., 0000-0001-5729-6517; X.D., 0000-0002-8968-0633

\*Correspondence: XW, [wangxueye@mail.iggcas.ac.cn](mailto:wangxueye@mail.iggcas.ac.cn); ZT, [tangzihua@mail.iggcas.ac.cn](mailto:tangzihua@mail.iggcas.ac.cn)

**Abstract:** As the junction of the Silk Roads, the Tarim Basin played a critical role in human migration and cultural interaction between the East and the West. Recently, population migration patterns have been increasingly reconstructed from strontium isotope ratios ( $^{87}\text{Sr}/^{86}\text{Sr}$ ) in archaeological human skeletons, and further constraints on their provenance require a bioavailable  $^{87}\text{Sr}/^{86}\text{Sr}$  map across the basin. Based on measurement data from 44 river samples in this study and 29 samples from published data, we generate the first map of bioavailable  $^{87}\text{Sr}/^{86}\text{Sr}$  values across the Tarim Basin and the neighbouring area. From the baseline map, three geologically distinct regions can be identified: (1) the Yili Block, Tian Shan orogenic belt and northern Tarim Block with lower ratios ( $0.7105 \pm 0.0007$  ( $1\sigma$ ),  $n = 25$ ); (2) the southern Tarim Block with higher ratios ( $0.7118 \pm 0.0008$ ,  $n = 29$ ); and (3) the eastern Pamir Block with diverse values ( $0.7110 \pm 0.0009$ ,  $n = 19$ ). This map is a promising tool for recognizing the origins of immigrants in the Tarim Basin and may aid understanding of the migration patterns and cultural communication along the Silk Roads.

Received 4 April 2018; revised 1 July 2018; accepted 3 July 2018

The Silk Roads were an interconnected web of routes linking trade centres from China to the Eastern Mediterranean and beyond (Kuzmina 2008; Liu 2010; Frchetti *et al.* 2017). They promoted cultural interaction and exchange across the Eurasian continent, contributing to the development of many of the world's great civilizations (Hansen 2012). At one of the critical positions on these roads, the Tarim Basin played a significant role in human migration and cultural communication between the East and the West (Li *et al.* 2010) (Fig. 1a). Understanding human migration patterns across the basin is therefore a key part in evaluating models of migration, trade and cultural interaction along the Silk Roads.

Recently, strontium (Sr) isotopes have been used in archaeological studies to reconstruct patterns of human migration (Ericson 1985; Bentley 2006). Strontium comes from weathering rocks, water and enters into the skeleton and dentition through the food chain without measurable fractionation (Blum *et al.* 2000). The  $^{87}\text{Sr}/^{86}\text{Sr}$  values in human enamel can thus reflect the local geology and are increasingly used to distinguish immigrants within a population (Copeland *et al.* 2011; Price *et al.* 2018).

A baseline map of  $^{87}\text{Sr}/^{86}\text{Sr}$  values throughout a region facilitates the evaluation of the source of immigrants (Beard & Johnson 2000; Laffoon *et al.* 2012; Hartman & Richards 2014). Several different approaches have been taken to establish  $^{87}\text{Sr}/^{86}\text{Sr}$  baseline maps at local and regional scales. One approach is to model  $^{87}\text{Sr}/^{86}\text{Sr}$  variations based on the bedrock lithology, age and weathering rates, which has been achieved in the USA (Beard & Johnson 2000; Bataille & Bowen 2012; Bataille *et al.* 2014; Crowley *et al.* 2017), the circum-Caribbean region (Bataille *et al.* 2012) and Western Europe (Bataille *et al.* 2018). Although the modelling approach has shown significant potential for mapping Sr isotopes over large areas, it requires high-resolution geological survey information and therefore is unlikely to become widely used.

The most commonly suggested approach is to measure Sr isotopes in directly sampled materials, such as rocks, soil leachates, surface and groundwater samples, plants and animal tissues (Maurer *et al.* 2012). This has been used to create baseline  $^{87}\text{Sr}/^{86}\text{Sr}$  maps in Mesoamerica (Hodell *et al.* 2004), North America (Brennan *et al.* 2014, 2016), Europe (Bentley & Knipper 2005; Montgomery *et al.* 2006; Evans *et al.* 2009, 2010; Frei & Frei 2011, 2013; Willmes *et al.* 2014, 2018) and Asia (Kusaka *et al.* 2011; Song *et al.* 2014). Among these materials, surface water – an important contributor of ingested Sr in humans and animals – provides an excellent estimate of the average bioavailable Sr isotope signals in the catchment areas and has been successfully used for mapping  $^{87}\text{Sr}/^{86}\text{Sr}$  ratios in Denmark and Britain, for example (Evans *et al.* 2010; Frei & Frei 2011, 2013).

To date, there is no baseline map characterizing the geographical distribution of  $^{87}\text{Sr}/^{86}\text{Sr}$  ratios across the Tarim Basin, hindering the use of  $^{87}\text{Sr}/^{86}\text{Sr}$  ratios for investigating archaeological provenance and human migration along the Silk Roads. Here, we analyse strontium isotope ratios of river water samples collected from the Tarim Basin and its surrounding area and generate the first map of bioavailable  $^{87}\text{Sr}/^{86}\text{Sr}$  signatures across the Tarim Basin, which allows for provenance studies along the Silk Roads.

## Geological setting

The Tarim Basin is bounded by the Tian Shan Mountains to the north, the western Kunlun Mountains to the south, the Altyn Tagh Mountains to the SE and the Pamir Plateau to the west. It is a hydrologically closed basin with rivers originating from the surrounding mountains and flowing into the basin interior. The basin and its neighbouring area can be geologically divided into several tectonic units: the Yili Block, the Tarim Block and the

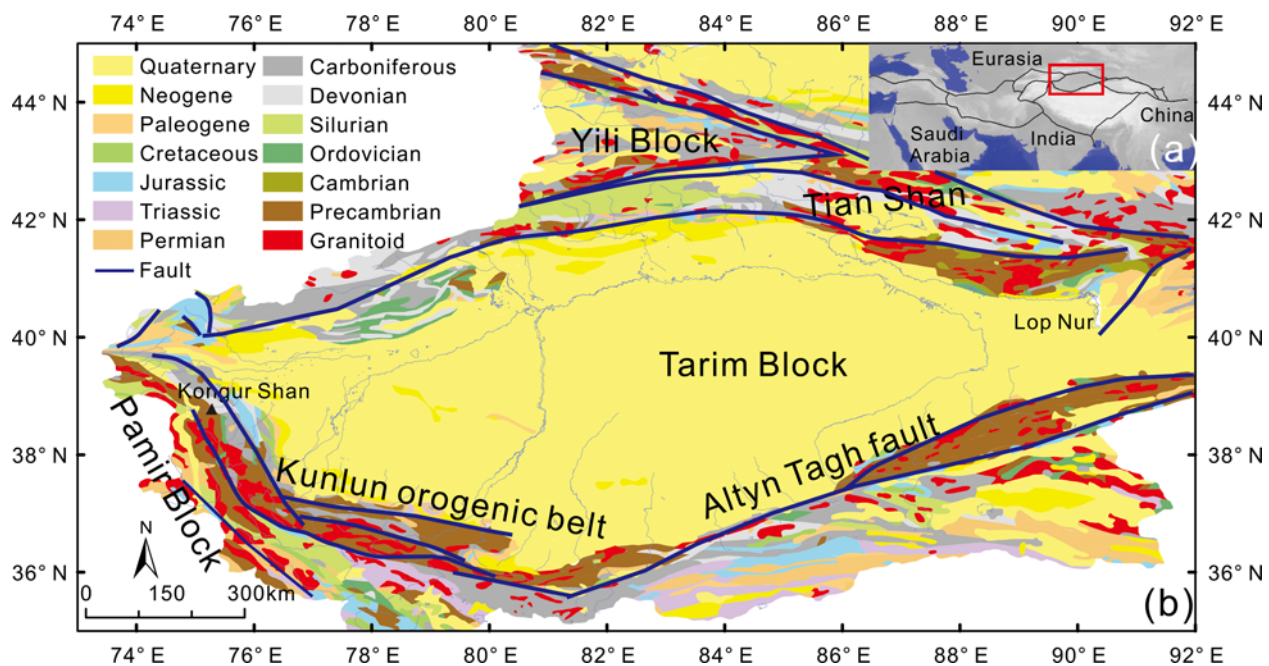


Fig. 1. (a) Sketch map of the Silk Roads showing major routes. (b) Simplified geological map of the study area (modified after Ma *et al.* 2002).

eastern Pamir Block, as well as the Tian Shan orogenic belt, the Kunlun orogenic belt and the Altyn Tagh fault along its margins (Wang 2006) (Fig. 1b).

The Yili Block is a triangular shape sandwiched within the Tian Shan orogenic belt (Wang *et al.* 2007). The interior of the block is dominated by Mesozoic–Cenozoic sedimentary rocks. In the eastern margins Carboniferous–Permian carbonate, clastic and volcanic rocks widely crop out, while in the south Carboniferous granitoids are exposed (Ma *et al.* 2002). Within the Tian Shan orogenic belt, Devonian–Carboniferous clastic and carbonate rocks are exposed in South Tian Shan. In contrast, Proterozoic metamorphic rocks, and Paleozoic granitoids and marine clastic rocks are widespread in regions north of South Tian Shan (Allen *et al.* 1999).

Bounded by diverse mountains, the basement of the Tarim Block predominantly consists of Archean and Proterozoic metamorphic rocks (Yang & Liu 2002) and is completely covered by clastic deposits eroded from the surrounding mountains. The northern Tarim Block is mainly covered by Paleozoic clastic and carbonate rocks eroded from South Tian Shan. In contrast, the SW Tarim Block is dominated by exposures of Proterozoic granitoids and metamorphic rocks, Carboniferous carbonate and clastic rocks, and Paleozoic granitoids, which crop out along the piedmont of the Kunlun Mountains (Zhang *et al.* 1995). The SE Tarim Block, on the north side of the Altyn Tagh fault, is covered by Proterozoic metamorphic rocks, Paleozoic carbonate rocks and a few Proterozoic granitoids. Quaternary deposits are widely distributed in the central Tarim Block (Ma *et al.* 2002).

The Pamir Block lies in the NW region of the Indo-Asian collision zone. As one of the most tectonically active regions in Central Asia (Cao *et al.* 2013), a variety of rocks are exposed in this block, including mainly Proterozoic gneisses, Paleozoic–Mesozoic metamorphic rocks, carbonate rocks and granitoids, and Cenozoic igneous and sedimentary rocks (Schwab *et al.* 2004).

## Material and methods

### Strontium isotope analysis

A total of 44 river water samples were collected from the Tarim Basin and its surroundings in 2016, including 4 samples from the Yili Basin, 3 samples within the Tian Shan orogenic belt, 13

samples from the northern Tarim Basin, 16 samples from the southern Tarim Basin and 8 samples from the eastern Pamir Plateau (Fig. 2). These samples were collected from rivers with abundant water discharge to maximize the representativeness of the river systems. The sampling sites were chosen carefully to avoid the influence of water pollution.

At each sample site, river water was collected in a 10 ml borosilicate bottle. After centrifuging the sample, approximately 5 ml of supernatant was dried on a hotplate at 100°C. All samples were dissolved in Teflon-PFA vials using 1.1 ml of 2.5 N HCl. Sr was separated from the matrix using AG50W×12 resin, an Sr-selective resin (200–400 mesh) loaded into the tip of a 2 ml Teflon column. The whole procedure blanks for Sr were typically lower than 200 pg. Isotopic ratios were measured on a Finnigan MAT262 thermal ionization mass spectrometer (TIMS) housed at the State Key Laboratory of Lithospheric Evolution at the Institute of Geology and Geophysics, Chinese Academy of Sciences (IGGCAS), using the internal ratio  $^{88}\text{Sr}/^{86}\text{Sr} = 8.375209$  to correct for mass fractionation. All measurements are referenced to a value of  $^{87}\text{Sr}/^{86}\text{Sr} = 0.710250$  for the NBS 987 standard, which was run concurrently with samples and yielded a mean  $^{87}\text{Sr}/^{86}\text{Sr}$  ratio of  $0.710266 \pm 0.000013$  ( $2\sigma$ ) in this work (Li *et al.* 2015).

Additionally, the  $^{87}\text{Sr}/^{86}\text{Sr}$  data of 29 published river water samples across the Tarim Basin were reanalysed, with the sampling sites including the northern Kunlun Mountains, the eastern Pamir Plateau, SW Tian Shan and the Lop Nur region in the eastern basin (Fig. 2) (Zhang *et al.* 1995; Liu *et al.* 1999; Tong *et al.* 2017).

### Kriging methods

The kriging interpolation method was used to generate a baseline map across the Tarim Basin based on the 44 river samples in this study and the data from the 29 published studies, and then cross-validation was performed to evaluate the quality of the map (Bro *et al.* 2008). During the validation step, we calculated the mean absolute error (MAE), root mean square error (RMSE) and residuals of the model, which are estimates of the spatial uncertainty to measure the predictive power of the tested model (Chai & Draxler 2014). The graphic representation was performed with Surfer software.

## Bioavailable Sr isotope map across the Tarim Basin

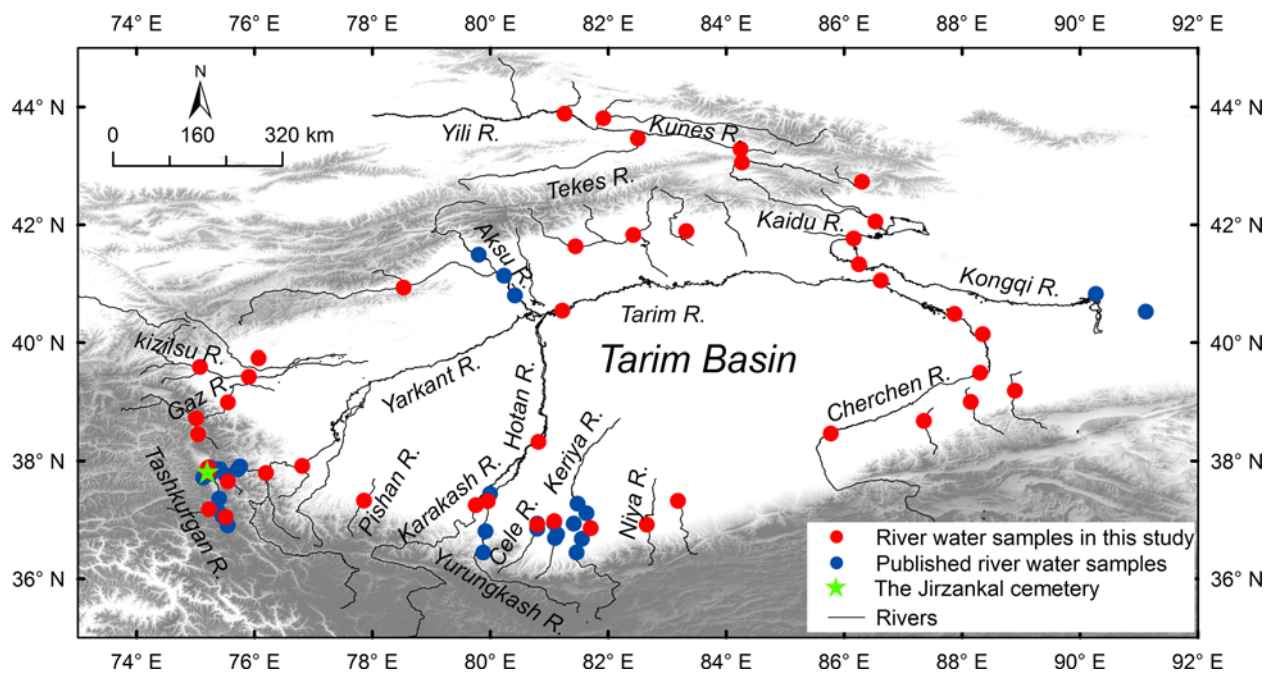


Fig. 2. Map of the Tarim Basin with localities of river water samples and published data (Zhang *et al.* 1995; Liu *et al.* 1999; Tong *et al.* 2017).

## Results

### $^{87}\text{Sr}/^{86}\text{Sr}$ ratios of the river water samples

The  $^{87}\text{Sr}/^{86}\text{Sr}$  ratios of 44 river water samples across the Tarim Basin show a wide range, from 0.70913 to 0.71339, with a mean of  $0.7111 \pm 0.0010$  ( $1\sigma$ ) (Table 1). The most radiogenic value we observed comes from the Pishan River watershed in the Kunlun Mountains and the lowest value from the Kizilsu River in SW Tian Shan.

### The first map of bioavailable $^{87}\text{Sr}/^{86}\text{Sr}$ distribution across the Tarim Basin

To better represent the geographical  $^{87}\text{Sr}/^{86}\text{Sr}$  distribution across the Tarim Basin, we performed kriging interpolation based on 73 river data to plot an isoline map (Fig. 3a) and used cross-validation to evaluate the quality of the kriging interpolation (Fig. 3b). The kriging interpolation results in a MAE of 0.0006 (13.4% of the whole  $^{87}\text{Sr}/^{86}\text{Sr}$  dataset range), an RMSE of 0.0008 (19.2% of the whole  $^{87}\text{Sr}/^{86}\text{Sr}$  dataset range) and low residuals (-0.001 to +0.001), indicating a good fit between the predicted and observed values. However, the residuals remain high in some areas because of the low sampling density, such as in Central Tian Shan.

The kriging interpolation provides the first detailed map for bioavailable  $^{87}\text{Sr}/^{86}\text{Sr}$  ratios across the Tarim Basin. It is clear that the  $^{87}\text{Sr}/^{86}\text{Sr}$  values across the basin exhibit a strong south–north gradient. The rivers draining the northern regions are less radiogenic than the rivers south of the Tarim Basin (Figs 3a, 4a). The rivers from the northern regions have a mean value of  $0.7105 \pm 0.0007$  ( $n = 25$ ), varying from 0.70913 to 0.71251, whereas the rivers south of the Tarim Basin have a mean value of  $0.7118 \pm 0.0008$  ( $n = 29$ ), varying from 0.71048 to 0.71349. An overlap exists in the  $^{87}\text{Sr}/^{86}\text{Sr}$  values between the rivers north and south of the study area, with extremely high values occurring in Central Tian Shan and low values occurring in part of the southern Tarim Basin (e.g. the Niya River). The Sr isotope ratios in the eastern Pamir Plateau ( $0.7110 \pm 0.0009$ ,  $n = 19$ ) display a complex distribution and have a large overlap with the ratios in the Tarim Basin.

### Inter- and intra-block variability

Inter- and intra-block variations in the  $^{87}\text{Sr}/^{86}\text{Sr}$  ratios are observed across the Tarim Basin (Fig. 4b). In the Yili Block, the  $^{87}\text{Sr}/^{86}\text{Sr}$

values of rivers are less radiogenic and show a wide range from 0.70922 to 0.71131 ( $0.7103 \pm 0.0009$ ,  $n = 4$ ). The most radiogenic values are observed in the southern tributary of the Yili River (Tekes River), whereas the eastern tributary of the Yili River (Kunes River) is less radiogenic. In regions of the Tian Shan orogenic belt, the  $^{87}\text{Sr}/^{86}\text{Sr}$  values range from 0.71033 to 0.71251, with a relatively high value of 0.71251 in the tributary of the Kaidu River draining Central Tian Shan, and low values in the main stream of the Kaidu River flowing through South Tian Shan (Fig. 3a).

There is an abrupt Sr isotope transition from the north to the southern Tarim Block. The rivers in the southern Tarim Block are much more radiogenic and encompass a wider range of  $^{87}\text{Sr}/^{86}\text{Sr}$  ratios than rivers in the northern Tarim Block. In the northern Tarim, river waters yield a lower mean of  $0.7105 \pm 0.0007$  ( $n = 13$ ) and exhibit a slight east–west gradient, whereas rivers draining SW Tian Shan ( $<0.7102$ ) are less radiogenic than rivers from the eastern block ( $>0.7105$ ) (e.g. the Lop Nur region). The Tarim River, the largest river in the Tarim Basin, presents homogeneous and low values in both the upper and lower reaches ( $0.7108 \pm 0.0001$ ). By contrast, relatively higher ratios pervade throughout the southern Tarim Block (a mean of 0.7118), the highest values ( $>0.712$ ) being in the northern piedmont of the Kunlun Mountains and the Altyn Tagh Mountains and gradually decreasing to lower values in the central Tarim Basin ( $<0.711$ ). Within the SW Tarim Block, the  $^{87}\text{Sr}/^{86}\text{Sr}$  ratios of the rivers vary from 0.71059 to 0.71349 ( $0.7119 \pm 0.0008$ ,  $n = 22$ ). The most radiogenic values are in river waters from the Pishan River, the Karakash River and the Cele River, while the values in the upper Yurungkash River (0.71059) are much lower than any other values in this block. Similarly, the  $^{87}\text{Sr}/^{86}\text{Sr}$  ratios within the SE block have a high average value of  $0.7115 \pm 0.0009$  ( $n = 7$ ), ranging from 0.71048 to 0.71312, whereas the Sr isotope ratio in the Niya River is exceptionally low (0.71048).

The  $^{87}\text{Sr}/^{86}\text{Sr}$  ratios of rivers in the eastern Pamir Block are heterogeneous, ranging from 0.71019 to 0.71293. There are mainly two distinct  $^{87}\text{Sr}/^{86}\text{Sr}$  groups in this region ( $\sim 0.710$ – $0.711$  and  $\sim 0.7115$ – $0.7125$ ). The lowest values occur in the middle and lower reaches of the Tashkurgan River ( $0.7105 \pm 0.0002$ ,  $n = 11$ ), which are much less radiogenic than the rivers throughout the entire area of the Tarim Basin. The highest values are observed in the upper Tashkurgan River ( $0.7116 \pm 0.0011$ ,  $n = 6$ ), as well as in the Kongur Shan and Muztaga massifs (0.71154–0.71239).

**Table 1.** *Strontium isotope compositions of the river water samples*

Block	Location	Sample name	Longitude	Latitude	$^{87}\text{Sr}/^{86}\text{Sr}$	Error (2 $\sigma$ )
Northern Tarim Block	westernmost part of central Tian Shan	16Hydro-01	76.08	39.75	0.71049	0.00001
SW Tarim Block	Gaz River	16Hydro-02	75.56	39.00	0.71191	0.00001
	Bulunkou Reservoir	16Hydro-03	75.02	38.73	0.71239	0.00001
	Karakul Lake	16Hydro-04	75.05	38.46	0.71154	0.00001
Eastern Pamir Block	Tashkurgan River	16Hydro-05	75.23	37.82	0.71044	0.00001
	Taheman River	16Hydro-06	75.22	37.89	0.71048	0.00001
	Bandier River	16Hydro-07	75.56	37.66	0.71071	0.00001
	Yarkant River	16Hydro-09	76.20	37.80	0.71070	0.00001
SW Tarim Block	Yarkant River	16Hydro-10	76.82	37.92	0.71076	0.00001
	Yili River	16Hydro-17	81.26	43.89	0.71038	0.00001
Yili block	Kash River	16Hydro-18	81.92	43.81	0.71018	0.00001
	Tekes River	16Hydro-19	82.51	43.47	0.71131	0.00001
	Kunes River	16Hydro-20	84.25	43.29	0.70922	0.00001
	upstream of the Kaidu River	16Hydro-21	84.27	43.06	0.71079	0.00001
Tian Shan orogenic belt	tributary of the Kaidu River	16Hydro-22	86.31	42.74	0.71251	0.00001
	Kaidu River	16Hydro-23	86.54	42.06	0.71033	0.00002
	Kongqi River	16Hydro-24	86.17	41.77	0.71056	0.00001
	Yaha River	16Hydro-25	83.33	41.89	0.71026	0.00001
Northern Tarim Block	Kizil River	16Hydro-27	82.43	41.83	0.71079	0.00001
	Muzhaerte River	16Hydro-29	81.45	41.64	0.71175	0.00001
	upstream of the Tarim River	16Hydro-30	81.23	40.54	0.71085	0.00001
	Hotan River	16Hydro-31	80.82	38.33	0.71181	0.00001
SW Tarim Block	Yurungkash River	16Hydro-32	79.97	37.32	0.71208	0.00001
	Karakash River	16Hydro-33	79.76	37.26	0.71287	0.00001
	Pishan River	16Hydro-34	77.86	37.33	0.71339	0.00001
	Kashgar River	16Hydro-35	75.91	39.43	0.70917	0.00001
Northern Tarim Block	Kizilsu River	16Hydro-36	75.08	39.60	0.70913	0.00001
	Toxkan River	16Hydro-37	78.54	40.94	0.71064	0.00001
Eastern Pamir Block	Kalaqigu River	16Hydro-42	75.24	37.18	0.71293	0.00001
	Taghdumbash River	16Hydro-46	75.52	37.05	0.71093	0.00001
	Kongqi River	16Hydro-48	86.26	41.33	0.71060	0.00001
Northern Tarim Block	downstream of the Tarim River	16Hydro-51	86.63	41.06	0.71081	0.00001
	downstream of the Tarim River	16Hydro-52	87.88	40.49	0.71076	0.00001
	downstream of the Tarim River	16Hydro-53	88.36	40.15	0.71075	0.00001
	Taitema Lake	16Hydro-54	88.31	39.50	0.71098	0.00001
	Miran River	16Hydro-55	88.90	39.20	0.71110	0.00001
	Ruoqiang River	16Hydro-56	88.16	39.01	0.71158	0.00001
SE Tarim Block	Waxxari River	16Hydro-57	87.36	38.69	0.71312	0.00001
	Cherchen River	16Hydro-58	85.78	38.47	0.71094	0.00001
	Yatongguz River	16Hydro-59	83.18	37.33	0.71159	0.00001
	Niya River	16Hydro-60	82.66	36.92	0.71048	0.00001
	Keriya River	16Hydro-61	81.71	36.86	0.71094	0.00001
SW Tarim Block	Damago River	16Hydro-62	81.09	36.98	0.71163	0.00001
	Cele River	16Hydro-63	80.80	36.92	0.71235	0.00001

## Discussion

By comparing the characterization of Sr isotopes in the rivers, we identify three regional patterns across the Tarim Basin: (1) the northern regions with lower ratios ( $0.7105 \pm 0.0007$ ,  $n = 25$ ), including the Yili Block, the Tian Shan orogenic belt and the northern Tarim Block; (2) the area south of the Tarim Block, with higher ratios ( $0.7118 \pm 0.0008$ ,  $n = 29$ ); and (3) the eastern Pamir Block with diverse values ( $0.7110 \pm 0.0009$ ,  $n = 19$ ).

### *Identifying sources of bioavailable strontium and baseline $^{87}\text{Sr}/^{86}\text{Sr}$ signatures*

The Sr isotopic compositions of rivers across the Tarim Basin are largely controlled by the geological signatures of their drainage areas (Zhang *et al.* 1995). As  $^{87}\text{Sr}/^{86}\text{Sr}$  values in rocks and minerals depend on their Rb/Sr values and geological age, Precambrian granitic rocks typically characterized by high Rb/Sr values tend to

have higher  $^{87}\text{Sr}/^{86}\text{Sr}$  ratios than areas with geologically younger rocks with low Rb/Sr values, such as Paleozoic carbonate rocks (Capo *et al.* 1998).

The Yili Block and northern Tarim Block are widely covered by Paleozoic carbonate rocks, Paleozoic–Cenozoic clastic rocks and Quaternary deposits, while Paleozoic granitoids and volcanic rocks are relatively scarce (Fig. 1). The  $^{87}\text{Sr}/^{86}\text{Sr}$  ratios in this region are expected to exhibit little variation and less radiogenic signatures. In particular, rivers draining SW Tian Shan show the lowest  $^{87}\text{Sr}/^{86}\text{Sr}$  ratios across the Tarim Basin, which are likely influenced by Devonian–Carboniferous clastic and carbonate rocks (Allen *et al.* 1999). In contrast, with the wide distribution of the Proterozoic–Paleozoic metamorphic and granitic terrains of the Kunlun Mountains and the Altyn Tagh Mountains, the rivers in the southern Tarim Basin show relatively higher  $^{87}\text{Sr}/^{86}\text{Sr}$  values than the rivers in the northern basin that are draining the relatively young area.

## Bioavailable Sr isotope map across the Tarim Basin

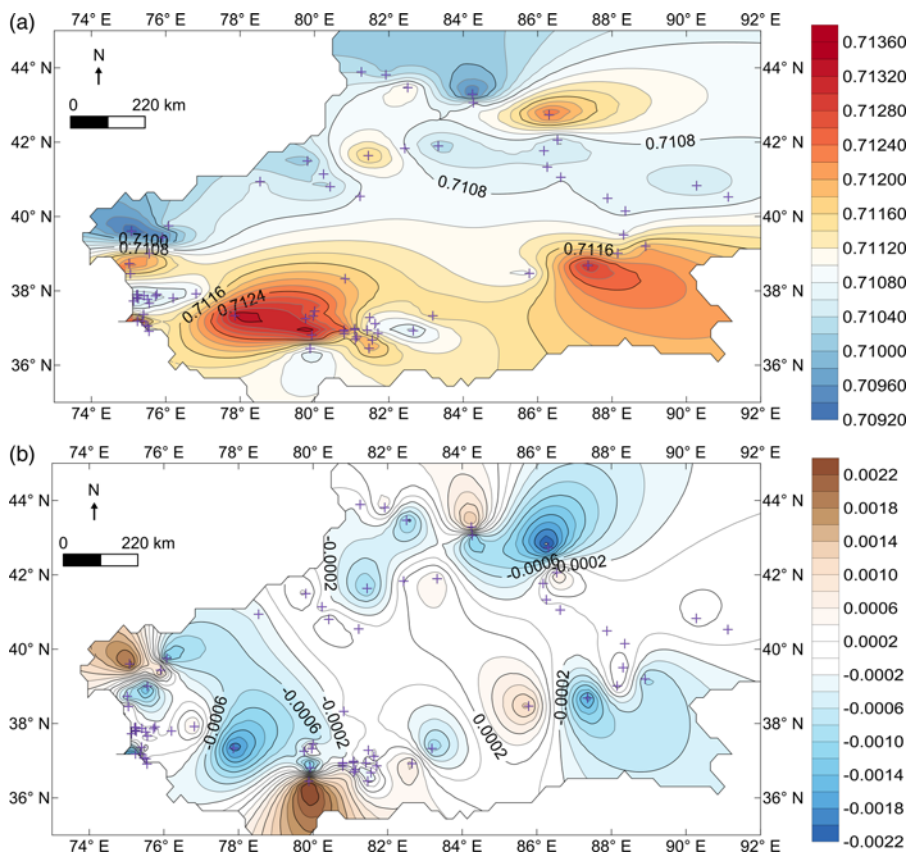


**Fig. 3.** (a) Geographical distribution of the  $^{87}\text{Sr}/^{86}\text{Sr}$  values of river samples based on kriging interpolation. (b) Residual analysis using cross-validation methods.

As one of the most tectonically active regions, the eastern Pamir Block is geologically diverse, including mainly Paleozoic–Cenozoic granitoids, Paleozoic–Mesozoic metamorphic and carbonate rocks, and Cenozoic igneous and sedimentary rocks.

The  $^{87}\text{Sr}/^{86}\text{Sr}$  ratios of river waters from this block exhibit greater variation than other blocks. The river waters in the middle and lower reaches of the Tashkurgan River have lower  $^{87}\text{Sr}/^{86}\text{Sr}$  ratios, which are mainly derived from the Permian–Triassic marine carbonate rocks with low values (Dufour *et al.* 2007; Ke *et al.* 2016). On the other hand, the rivers originating from the Kongur Shan and Muztaga massifs show higher Sr isotope ratios, reflecting the influence of the Paleozoic–Mesozoic granitoids and metamorphic rocks in these areas (Robinson *et al.* 2007; Zhang *et al.* 2016). Other high values occurring in the upper Tashkurgan River are probably influenced by the Mesozoic granitoids (Ma *et al.* 2002).

Although rivers north and south of the Tarim Basin have distinct Sr isotope ratios, several exceptional ratios exist in the basin and the neighbouring area. For example, a few elevated  $^{87}\text{Sr}/^{86}\text{Sr}$  values are observed in the northern regions, such as the Tekes River in the Yili Block (0.71131), the Muzhaerte River in South Tian Shan (0.71176) and a tributary of the Kaidu River (0.71251), which may possibly be derived from Proterozoic metamorphic rocks and Paleozoic granitoids in their catchment areas (Ma *et al.* 2002). Additionally, the Niya River and the upper Yurungkash River in the southern Tarim Block have extremely low values ( $<0.7106$ ), indicating that carbonate weathering may be more influential in the local areas, as Carboniferous carbonate rocks are partly exposed in the Kunlun Mountains.

The major ion composition data from these rivers further support the interpretation of Sr sources (Fig. 5). The rivers from the northern regions mostly have high concentrations of  $\text{Ca}^{2+} + \text{Mg}^{2+}$  and  $\text{HCO}_3^-$ , low Na/Ca, Mg/Ca and K/Ca molar ratios (Zhang *et al.* 1995), and somewhat high concentrations of  $\text{Na}^+ + \text{K}^+$  and  $\text{Cl}^- + \text{SO}_4^{2-}$ , indicating influences from carbonate weathering and partly from evaporite dissolution ( $^{87}\text{Sr}/^{86}\text{Sr}$  of evaporites  $<0.7108$  in the northern basin; Wang *et al.* 2015). In the southern Tarim Block,  $\text{Na}^+ + \text{K}^+$  and  $\text{Cl}^-$  are dominant in most rivers, and the cation concentration ratios are in agreement with the silicate end-member (Zhang *et al.* 1995), reflecting a significant contribution from

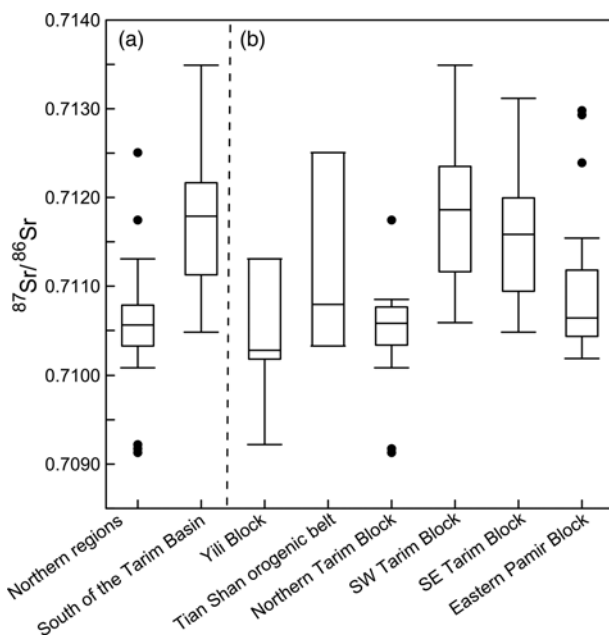


**Fig. 4.** Box-plots illustrating the distribution of  $^{87}\text{Sr}/^{86}\text{Sr}$  ratios in 73 river water samples across the Tarim Basin (bold horizontal line signifies median, box extent signifies quartiles 25% and 75%, solid line represents non-outlier range, black-filled circle represents outlier). (a) Rivers from the northern regions (including the Yili Basin, Tian Shan and northern Tarim Basin) and southern Tarim Block. (b) Inter- and intra-block  $^{87}\text{Sr}/^{86}\text{Sr}$  variations.

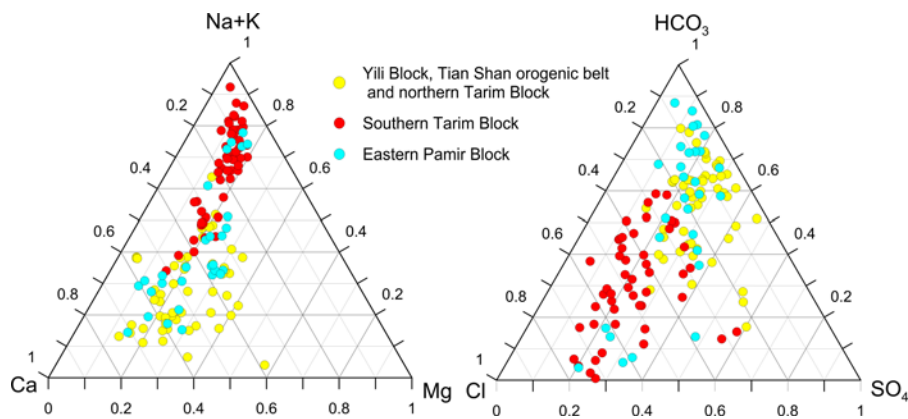


**Fig. 5.** Ternary diagrams for cations and anions in river waters across the Tarim Basin. The data were collected from published studies (Zhang *et al.* 1995; Zhu & Yang 2007; Zhu *et al.* 2011; Xiao *et al.* 2012; Wu 2016; Tong *et al.* 2017).

evaporite dissolution ( $^{87}\text{Sr}/^{86}\text{Sr}$  of evaporites  $\sim 0.7115$  in the southern basin; Zhang *et al.* 1995) and silicate weathering (e.g. granitoids). Therefore, rivers in the south of the basin are more influenced by evaporite dissolution and silicate weathering and thus more radiogenic than rivers in the northern region, which are influenced by carbonate weathering. The complex ion distribution shown in the Ternary diagrams may indicate that the rivers in the eastern Pamir Block are derived from mixed sources, complicating the distribution of Sr isotopes in this block.

### Implications of the results for the Jirzankal site

The Jirzankal cemetery (*c.* 2.5 ka BP) is located on the western bank of the Tashkurgan River, eastern Pamir Plateau (Fig. 2). While most human enamel  $^{87}\text{Sr}/^{86}\text{Sr}$  values ( $0.71043 \pm 0.00022$ ,  $n = 34$ ; Wang *et al.* 2016) measured in the cemetery coincide with the range of river waters collected from the Tashkurgan River ( $0.71044 \pm 0.00015$ ,  $n = 6$ ), two individuals from graves M1 and M14 show lower values (0.70997 and 0.71004). These signatures are exceptionally low when compared to the range from the eastern Pamir Block, which may indicate that these two individuals grew up beyond the eastern Pamir Block, and possibly outside of the Tarim Basin. On the baseline map presented above, the areas with similar  $^{87}\text{Sr}/^{86}\text{Sr}$  values might be their possible sources, including SW Tian Shan ( $< 0.7102$ ). The possibility that these individuals may have migrated in from regions beyond the study area cannot be excluded because no accurate provenance can be identified solely on the strontium isotope baseline map. Therefore, future work will turn to other systems (e.g. oxygen and lead isotopes) in the same samples to place more constraints. Many exotic mortuary objects are found in the Jirzankal cemetery, such as silk fabrics from grave M1 and an angular harp in grave M14. Both of these objects originated far from the Pamir Plateau, implying the existence of cross-continental trade. This also calls for a higher sample density and broader coverage to enlarge this baseline map, particularly outside the Tarim Basin.

### Conclusions

In this study, we analyse the Sr isotope ratios of river waters collected from the Tarim Basin and its surrounding area, and construct the first baseline map of  $^{87}\text{Sr}/^{86}\text{Sr}$  values across the Tarim Basin. This provides a powerful tool for archaeological provenance studies.

A large spatial variation in  $^{87}\text{Sr}/^{86}\text{Sr}$  ratios exists in rivers across the Tarim Basin, which allows division of the basin into three regions. Rivers south of the Tarim Basin exhibit higher and more variable ratios than rivers north, while eastern Pamir, with its diverse geology, has overlaps in  $^{87}\text{Sr}/^{86}\text{Sr}$  ratios with the other two regions. This pattern might result from differences in Sr sources.

As geological information and geochemical data suggest, the Sr isotopes in the southern rivers are mainly derived from metamorphic rocks and granitoids sources, whereas the northern rivers are more influenced by carbonate rocks.

Although the baseline map at this stage is still preliminary, it has shown the potential to interpret strontium isotope data obtained from ancient human remains in this region. Hopefully it will further contribute to understanding human migration patterns along the Silk Roads after improvements in the sampling density and the scope of the study area.

**Acknowledgements** We thank Despina Zoura from the University of Leeds for field assistance and Ms Li Youlian and Prof. Li Chaofeng for their laboratory guidance. In addition, we are indebted to the editor, Graham Shields-Zhou, Jane Evans and another anonymous reviewer for their constructive comments, which greatly improved the manuscript.

**Funding** This work was funded by the Strategic Priority Research Program of the Chinese Academy of Sciences (XDB26020401), the National Natural Science Foundation of China (41472151; 41672177) and the Ministry of Science and Technology of the People's Republic of China (2014FY210500).

*Scientific editing by Graham Shields-Zhou*

### References

- Allen, M.B., Vincent, S.J. & Wheeler, P.J. 1999. Late Cenozoic tectonics of the Kepingtage thrust zone: Interactions of the Tien Shan and Tarim Basin, northwest China. *Tectonics*, **18**, 639–654, <https://doi.org/10.1029/1999tc900019>
- Bataille, C.P. & Bowen, G.J. 2012. Mapping  $^{87}\text{Sr}/^{86}\text{Sr}$  variations in bedrock and water for large scale provenance studies. *Chemical Geology*, **304–305**, 39–52, <https://doi.org/10.1016/j.chemgeo.2012.01.028>
- Bataille, C.P., Laffoon, J. & Bowen, G.J. 2012. Mapping multiple source effects on the strontium isotopic signatures of ecosystems from the circum-Caribbean region. *Ecosphere*, **3**, 118, <https://doi.org/10.1890/es12-00155.1>
- Bataille, C.P., Brennan, S.R., Hartmann, J., Moosdorf, N., Wooller, M.J. & Bowen, G.J. 2014. A geostatistical framework for predicting variations in strontium concentrations and isotope ratios in Alaskan rivers. *Chemical Geology*, **389**, 1–15, <https://doi.org/10.1016/j.chemgeo.2014.08.030>
- Bataille, C.P., von Holstein, I.C.C., Laffoon, J.E., Willmes, M., Liu, X.M. & Davies, G.R. 2018. A bioavailable strontium isoscape for Western Europe: A machine learning approach. *PLoS One*, **13**, e0197386, <https://doi.org/10.1371/journal.pone.0197386>
- Beard, B.L. & Johnson, C.M. 2000. Strontium isotope composition of skeletal material can determine the birth place and geographic mobility of humans and animals. *Journal of Forensic Science*, **45**, 1049–1061, <https://doi.org/10.1520/JFS14829J>
- Bentley, R.A. 2006. Strontium isotopes from the earth to the archaeological skeleton: a review. *Journal of Archaeological Method and Theory*, **13**, 135–187, <https://doi.org/10.1007/s10816-006-9009-x>
- Bentley, R.A. & Knipper, C. 2005. Geographical patterns in biologically available strontium, carbon and oxygen isotope signatures in prehistoric SW Germany\*. *Archaeometry*, **47**, 629–644, <https://doi.org/10.1111/j.1475-4754.2005.00223.x>

## Bioavailable Sr isotope map across the Tarim Basin

- Blum, J.D., Talianferro, E.H., Weisse, M.T. & Holmes, R.T. 2000. Changes in Sr/Ca, Ba/Ca and  $^{87}\text{Sr}/^{86}\text{Sr}$  ratios between trophic levels in two forest ecosystems in the northeastern U.S.A. *Biogeochemistry*, **49**, 87–101, <https://doi.org/10.1023/a:1006390707989>
- Brennan, S.R., Fernandez, D.P., Mackey, G., Cerling, T.E., Bataille, C.P., Bowen, G.J. & Wooller, M.J. 2014. Strontium isotope variation and carbonate versus silicate weathering in rivers from across Alaska: Implications for provenance studies. *Chemical Geology*, **389**, 167–181, <https://doi.org/10.1016/j.chemgeo.2014.08.018>
- Brennan, S.R., Torgersen, C.E., Hollenbeck, J.P., Fernandez, D.P., Jensen, C.K. & Schindler, D.E. 2016. Dendritic network models: Improving isoscapes and quantifying influence of landscape and in-stream processes on strontium isotopes in rivers. *Geophysical Research Letters*, **43**, 5043–5051, <https://doi.org/10.1002/2016gl068904>
- Bro, R., Kjeldahl, K., Smilde, A.K. & Kiess, H.A. 2008. Cross-validation of component models: a critical look at current methods. *Analytical and Bioanalytical Chemistry*, **390**, 1241–1251, <https://doi.org/10.1007/s00216-007-1790-1>
- Cao, K., Bernet, M., Wang, G.C., van der Beek, P., Wang, A., Zhang, K.X. & Enkelmann, E. 2013. Focused Pliocene–Quaternary exhumation of the Eastern Pamir domes, western China. *Earth and Planetary Science Letters*, **363**, 16–26, <https://doi.org/10.1016/j.epsl.2012.12.023>
- Capo, R.C., Stewart, B.W. & Chadwick, O.A. 1998. Strontium isotopes as tracers of ecosystem processes: theory and methods. *Geoderma*, **82**, 197–225, [https://doi.org/10.1016/s0016-7061\(97\)00102-x](https://doi.org/10.1016/s0016-7061(97)00102-x)
- Chai, T. & Draxler, R.R. 2014. Root mean square error (RMSE) or mean absolute error (MAE)? – Arguments against avoiding RMSE in the literature. *Geoscientific Model Development*, **7**, 1247–1250, <https://doi.org/10.5194/gmd-7-1247-2014>
- Copeland, S.R., Sponheimer, M. *et al.* 2011. Strontium isotope evidence for landscape use by early hominins. *Nature*, **474**, 76–78, <https://doi.org/10.1038/nature10149>
- Crowley, B.E., Miller, J.H. & Bataille, C.P. 2017. Strontium isotopes ( $^{87}\text{Sr}/^{86}\text{Sr}$ ) in terrestrial ecological and palaeoecological research: empirical efforts and recent advances in continental-scale models. *Biological Reviews*, **92**, 43–59, <https://doi.org/10.1111/brv.12217>
- Dufour, M.S., Kol'tsov, A.B., Zolotarev, A.A. & Kuznetsov, A.B. 2007. Corundum-bearing metasedimentary rocks in the Central Pamirs. *Petrology*, **15**, 151–167, <https://doi.org/10.1134/s0869591107020038>
- Ericson, J.E. 1985. Strontium isotope characterization in the study of prehistoric human ecology. *Journal of Human Evolution*, **14**, 503–514, [https://doi.org/10.1016/S0047-2484\(85\)80029-4](https://doi.org/10.1016/S0047-2484(85)80029-4)
- Evans, J.A., Montgomery, J. & Wildman, G. 2009. Isotope domain mapping of  $^{87}\text{Sr}/^{86}\text{Sr}$  biosphere variation on the Isle of Skye, Scotland. *Journal of the Geological Society, London*, **166**, 617–631, <https://doi.org/10.1144/0016-76492008-043>
- Evans, J.A., Montgomery, J., Wildman, G. & Boulton, N. 2010. Spatial variations in biosphere  $^{87}\text{Sr}/^{86}\text{Sr}$  in Britain. *Journal of the Geological Society, London*, **167**, 1–4, <https://doi.org/10.1144/0016-76492009-090>
- Frachetti, M.D., Smith, C.E., Traub, C.M. & Williams, T. 2017. Nomadic ecology shaped the highland geography of Asia's Silk Roads. *Nature*, **543**, 193–198, <https://doi.org/10.1038/nature21696>
- Frei, K.M. & Frei, R. 2011. The geographic distribution of strontium isotopes in Danish surface waters – A base for provenance studies in archaeology, hydrology and agriculture. *Applied Geochemistry*, **26**, 326–340, <https://doi.org/10.1016/j.apgeochem.2010.12.006>
- Frei, R. & Frei, K.M. 2013. The geographic distribution of Sr isotopes from surface waters and soil extracts over the island of Bornholm (Denmark) – A base for provenance studies in archaeology and agriculture. *Applied Geochemistry*, **38**, 147–160, <https://doi.org/10.1016/j.apgeochem.2013.09.007>
- Hansen, V. 2012. *The Silk Road: A New History*. Oxford University Press, New York.
- Hartman, G. & Richards, M. 2014. Mapping and defining sources of variability in bioavailable strontium isotope ratios in the Eastern Mediterranean. *Geochimica et Cosmochimica Acta*, **126**, 250–264, <https://doi.org/10.1016/j.gca.2013.11.015>
- Hodell, D.A., Quinn, R.L., Brenner, M. & Kamenov, G. 2004. Spatial variation of strontium isotopes ( $^{87}\text{Sr}/^{86}\text{Sr}$ ) in the Maya region: a tool for tracking ancient human migration. *Journal of Archaeological Science*, **31**, 585–601, <https://doi.org/10.1016/j.jas.2003.10.009>
- Ke, S., Teng, F.Z., Li, S.G., Gao, T., Liu, S.A., He, Y.S. & Mo, X.X. 2016. Mg, Sr, and O isotope geochemistry of syenites from northwest Xinjiang, China: Tracing carbonate recycling during Tethyan oceanic subduction. *Chemical Geology*, **437**, 109–119, <https://doi.org/10.1016/j.chemgeo.2016.05.002>
- Kusaka, S., Nakano, T., Yumoto, T. & Nakatsukasa, M. 2011. Strontium isotope evidence of migration and diet in relation to ritual tooth ablation: a case study from the Inariyama Jomon site, Japan. *Journal of Archaeological Science*, **38**, 166–174, <https://doi.org/10.1016/j.jas.2010.09.001>
- Kuzmina, E.E. 2008. *The Prehistory of the Silk Road*. University of Pennsylvania Press, Philadelphia.
- Laffoon, J.E., Davies, G.R., Hoogland, M.L.P. & Hofman, C.L. 2012. Spatial variation of biologically available strontium isotopes ( $^{87}\text{Sr}/^{86}\text{Sr}$ ) in an archipelagic setting: a case study from the Caribbean. *Journal of Archaeological Science*, **39**, 2371–2384, <https://doi.org/10.1016/j.jas.2012.02.002>
- Li, C.F., Guo, J.H., Chu, Z.Y., Feng, L.J. & Wang, X.C. 2015. Direct high-precision measurements of the  $^{87}\text{Sr}/^{86}\text{Sr}$  isotope ratio in natural water without chemical separation using thermal ionization mass spectrometry equipped with 1012  $\Omega$  resistors. *Analytical Chemistry*, **87**, 7426–7432, <https://doi.org/10.1021/acs.analchem.5b01627>
- Li, C.X., Li, H.J. *et al.* 2010. Evidence that a West–East admixed population lived in the Tarim Basin as early as the early Bronze Age. *BMC Biology*, **8**, 15, <https://doi.org/10.1186/1741-7007-8-15>
- Liu, C.L., Wang, M.L. & Jiao, P.C. 1999. Hydrogen, oxygen, strontium and sulfur isotope geochemistry and potash-forming material sources of Lop salt lake, Xinjiang. *Mineral Deposits*, **18**, 268–275 [in Chinese with English abstract].
- Liu, X. 2010. *The Silk Road in World History*. Oxford University Press, New York.
- Ma, L.F., Qiao, X.F. & Liu, N.L. 2002. *Geological Atlas of China*. Geological Publishing House, Beijing [in Chinese].
- Maurer, A.F., Galer, S.J. *et al.* 2012. Bioavailable  $^{87}\text{Sr}/^{86}\text{Sr}$  in different environmental samples—effects of anthropogenic contamination and implications for isoscapes in past migration studies. *Science of the Total Environment*, **433**, 216–229, <https://doi.org/10.1016/j.scitotenv.2012.06.046>
- Montgomery, J., Evans, J.A. & Wildman, G. 2006.  $^{87}\text{Sr}/^{86}\text{Sr}$  isotope composition of bottled British mineral waters for environmental and forensic purposes. *Applied Geochemistry*, **21**, 1626–1634, <https://doi.org/10.1016/j.apgeochem.2006.07.002>
- Price, T.D., Arcini, C., Gustin, I., Drenzel, L. & Kalmring, S. 2018. Isotopes and human burials at Viking Age Birka and the Mälaren region, east central Sweden. *Journal of Anthropological Archaeology*, **49**, 19–38, <https://doi.org/10.1016/j.jaa.2017.10.002>
- Robinson, A.C., Yin, A., Manning, C.E., Harrison, T.M., Zhang, S.H. & Wang, X.F. 2007. Cenozoic evolution of the eastern Pamir: Implications for strain-accommodation mechanisms at the western end of the Himalayan–Tibetan orogen. *Geological Society of America Bulletin*, **119**, 882–896, <https://doi.org/10.1130/b25981.1>
- Schwab, M., Ratschbacher, L. *et al.*, 2004. Assembly of the Pamirs: Age and origin of magmatic belts from the southern Tien Shan to the southern Pamirs and their relation to Tibet. *Tectonics*, **23**, TC4002, <https://doi.org/10.1029/2003tc001583>
- Song, B.Y., Ryu, J.S., Shin, H.S. & Lee, K.S. 2014. Determination of the source of bioavailable Sr using  $^{87}\text{Sr}/^{86}\text{Sr}$  tracers: a case study of hot pepper and rice. *Journal of Agricultural and Food Chemistry*, **62**, 9232–9238, <https://doi.org/10.1021/jf503498r>
- Tong, X.X., Ma, W.M. & Sun, X.L. 2017. Characteristic and environmental significance of strontium isotope in glacial meltwater of the Tashkurgan area in Pamirs, Xinjiang. *Environmental Chemistry*, **36**, 830–838 [in Chinese with English abstract].
- Wang, B., Chen, Y. *et al.* 2007. Primary Carboniferous and Permian paleomagnetic results from the Yili Block (NW China) and their implications on the geodynamic evolution of Chinese Tianshan Belt. *Earth and Planetary Science Letters*, **263**, 288–308, <https://doi.org/10.1016/j.epsl.2007.08.037>
- Wang, F.T. 2006. *The Paleogeographic and Geo-ecological Atlas of Xinjiang Uygur Autonomous Region*. SinoMaps Press, Beijing [in Chinese].
- Wang, X.Y., Yin, H.W., Deng, X.L. & Wei, Z. 2015. Strontium isotope characteristics and the origin of Cenozoic salt deposits in Kuqa depression. *Journal of Nanjing University (Natural Science)*, **51**, 1068–1074 [in Chinese with English abstract].
- Wang, X.Y., Tang, Z.H., Wu, J., Wu, X.H., Wu, Y.Q. & Zhou, X.Y. 2016. Strontium isotope evidence for a highly mobile population on the Pamir Plateau 2500 years ago. *Scientific Reports*, **6**, 35162, <https://doi.org/10.1038/srep35162>
- Willmes, M., McMorro, L. *et al.* 2014. The IRHUM (Isotopic Reconstruction of Human Migration) database – bioavailable strontium isotope ratios for geochemical fingerprinting in France. *Earth System Science Data*, **6**, 117–122, <https://doi.org/10.5194/essd-6-117-2014>
- Willmes, M., Bataille, C.P. *et al.* 2018. Mapping of bioavailable strontium isotope ratios in France for archaeological provenance studies. *Applied Geochemistry*, **90**, 75–86, <https://doi.org/10.1016/j.apgeochem.2017.12.025>
- Wu, W.H. 2016. Hydrochemistry of inland rivers in the north Tibetan Plateau: Constraints and weathering rate estimation. *Science of the Total Environment*, **541**, 468–482, <https://doi.org/10.1016/j.scitotenv.2015.09.056>
- Xiao, J., Jin, Z.D., Ding, H., Wang, J. & Zhang, F. 2012. Geochemistry and solute sources of surface waters of the Tarim River Basin in the extreme arid region, NW Tibetan Plateau. *Journal of Asian Earth Sciences*, **54–55**, 162–173, <https://doi.org/10.1016/j.jseas.2012.04.009>
- Yang, Y.Q. & Liu, M. 2002. Cenozoic deformation of the Tarim plate and the implications for mountain building in the Tibetan Plateau and the Tian Shan. *Tectonics*, **21**, 1059, <https://doi.org/10.1029/2001tc001300>
- Zhang, J., Takahashi, K., Wushiki, H., Yabuki, S., Xiong, J.M. & Masuda, A. 1995. Water geochemistry of the rivers around the Taklimakan Desert (NW China): Crustal weathering and evaporation processes in arid land. *Chemical Geology*, **119**, 225–237, [https://doi.org/10.1016/0009-2541\(94\)00088-P](https://doi.org/10.1016/0009-2541(94)00088-P)
- Zhang, Q.C., Liu, Y., Huang, H., Wu, Z.H. & Zhou, Q. 2016. Petrogenesis and tectonic implications of the high-K Alamas calc-alkaline granitoids at the northwestern margin of the Tibetan Plateau: Geochemical and Sr–Nd–Hf–O

X. Wang *et al.*

- isotope constraints. *Journal of Asian Earth Sciences*, **127**, 137–151, <https://doi.org/10.1016/j.jseaes.2016.05.026>
- Zhu, B.Q. & Yang, X.P. 2007. The ion chemistry of surface and ground waters in the Taklimakan Desert of Tarim Basin, western China. *Chinese Science Bulletin*, **52**, 2123–2129.
- Zhu, B.Q., Yang, X.P., Rioual, P., Qin, X.G., Liu, Z.T., Xiong, H.G. & Yu, J.J. 2011. Hydrogeochemistry of three watersheds (the Erlqis, Zhungarer and Yili) in northern Xinjiang, NW China. *Applied Geochemistry*, **26**, 1535–1548, <https://doi.org/10.1016/j.apgeochem.2011.06.018>